

**Atom deposition and sputtering at normal incidence simulated by the Frenkel-Kontorova chain**D. U. Abdullina,<sup>1,\*</sup> Yu. V. Bebikhov<sup>2,†</sup> M. V. Khazimullin,<sup>1,2,‡</sup> A. A. Kudreyko<sup>3,§</sup> and S. V. Dmitriev<sup>1,4,||</sup><sup>1</sup>*Institute of Molecule and Crystal Physics, Ufa Federal Research Centre of Russian Academy of Sciences, 450075 Ufa, Russia*<sup>2</sup>*Polytechnic Institute (Branch) in Mirny, North-Eastern Federal University, 678170 Mirny, Sakha Republic (Yakutia), Russia*<sup>3</sup>*Department of Medical Physics and Informatics, Bashkir State Medical University, 450008 Ufa, Russia*<sup>4</sup>*Ufa State Petroleum Technological University, 450064 Ufa, Russia*

(Received 16 May 2022; accepted 28 July 2022; published 17 August 2022)

The impact of a molecule of  $N$  atoms with a speed of  $v_0$  on the free end of the Frenkel-Kontorova chain is numerically simulated. Depending on the values of  $N$  and  $v_0$ , different scenarios of the molecule-chain interaction are observed. Molecules with low speed stick to the chain. At somewhat higher speeds, the molecules bounce off the chain. Further increase in  $v_0$  results in bouncing off a molecule larger than the incident one. At even higher speed, bouncing of the molecule off the chain takes place simultaneously with the formation of a supersonic crowdion (antikink) propagating along the chain. A very high collision velocity leads to the sputtering of atoms from the chain and the formation of single and multiple supersonic crowdions. Interestingly, the sputtering yield  $Y$  as the function of  $v_0$  demonstrates a nonmonotonous dependence. This is explained by the fact that supersonic crowdions can have a discrete set of propagation velocities. When  $v_0$  is such that supersonic crowdions are effectively excited, the latter transfer energy deep into the chain, and the sputtering is minimal. For some  $v_0$  ranges, the formation of supersonic crowdions is suppressed. In these cases, the energy transferred from the impact of the molecule to the chain is spent mainly on the sputtering of atoms. The results obtained qualitatively explain the physics of bombardment of a crystal surface by atomic clusters with applications in physical vapor deposition, ion implantation, ion-beam sputtering, and similar experimental techniques.

DOI: [10.1103/PhysRevE.106.024207](https://doi.org/10.1103/PhysRevE.106.024207)**I. INTRODUCTION**

Ion beams with different energies can be used for shaping [1–4], testing [5–7], synthesizing [1,8], and modifying the properties [8–10] of materials, as summarized in the reviews such as References [1,11–13]. The interaction of accelerated ions with the crystal surface is quite complex, especially for high-energy ion beams. For the so-called linear collision cascades, when a low density of point defects is generated [12,14], the problem is simplified and can be solved using classical physical models. Cascades in metals are close to linear when bombarded by ions with energies below 10 keV [12].

Atomic layer deposition is a thin film deposition process known for its ability to create layers of controlled thickness and composition [15].

Sputtering is a process in which atoms or atomic clusters of a solid material are ejected from its surface by incident ions or particles [11,12].

Bombardment of the surface with low-energy ions (from 10 eV and above) leads to their deposition [15]. If surface

activation is required, then higher-energy ions, up to 5 keV, can be used for deposition of atomic layers.

Reviews of experimental work on the erosion of Be and beryllium ceramics by bombardment with hydrogen isotopes and various ions are reported in Refs. [16,17]. The energy dependence of the Be-sputtering yield due to bombardment by  $\text{Be}^+$  ions in the energy range of 1.5–10 keV at normal incidence was measured [18]. The yield is maximal at the ion energy of 1.5 keV, being equal to about 0.3 atoms per ion; further increase in the energy leads to a monotonous decrease of the yield. In the work [19] the ion-induced sputtering yields from monatomic solids at normal incidence are presented for various ion-target combinations in a range of the incident ion energy. Self-sputtering is sputtering with ionized atoms, the same as the target. Typically, the self-sputtering yield reaches its maximum at ion energies from 1 to 10 keV, with maximum values from 1 to several atoms per ion. Self-sputtering of copper is often used for copper deposition [20–22].

It has been experimentally established that the sputtering efficiency of materials depends relatively weakly on the mass of incident ions, with the exception of extremely light ions such as helium and hydrogen isotopes [19]. At a qualitative level, for not very high ion energies, this fact was explained in molecular dynamics calculations for Lennard-Jones bcc [23] and fcc [24] crystals.

Recently, argon cluster ion sources have been developed for surface analysis and treatment and are now widely used for surface cleaning and modification [25,26]. There are still insufficient data in the literature on the comparison of

\* dina.abdullina25@gmail.com

† bebikhov.yura@mail.ru

‡ maximhk@gmail.com

§ alexkudreyko@mail.ru

|| dmitriev.sergey.v@gmail.com

sputtering by ions and ionized clusters. Let us note several works on molecular dynamics modeling of the details of the process of cluster ion sputtering [27–30]. In particular, in Ref. [30] simulation of Ar cluster impact on silicon (001) surface has been conducted for clusters containing from 30 to 3000 atoms, and energy from 5 to 40 eV per atom. The model for total sputter yield estimation has been offered.

Point defects play a very important role in the structure relaxation of the materials under irradiation or ion beam treatment [14]. Interstitial atoms, compared to vacancies, have a higher formation energy but a lower migration energy. Interstitials in the form of crowdions have a very low migration energy and, therefore, a high migration ability, which makes their experimental analysis difficult [31]. For this reason, structure and motion of crowdions are often analyzed using computer simulation techniques such as molecular dynamics [32–35], Monte Carlo [36,37], multiscale [38–40], and *ab initio* [41,42] modeling.

Crowdions can move along close-packed atomic rows with subsonic or even supersonic speed. Static or subsonic crowdions have been well studied [40,41,43,44]. The supersonic crowdions (or antikinks) were studied with the help of one-dimensional Klein-Gordon lattices [45–47], two-dimensional Morse lattice [48,49], bcc [50], and fcc lattices [42,51,52].

Moving crowdions transfer mass and energy, playing an important role in the structural transformation of materials during high-energy impacts. It has been shown that the supersonic  $N$ -crowdions (multiple antikinks) transport energy more efficiently since they can be excited with a lower energy and travel longer distance than supersonic 1-crowdions (single antikinks) [45–48,51,52]. Supersonic 2-crowdions can be excited by bombarding the crystal surface with molecules [47,52].

In our recent work [47], the Frenkel-Kontorova chain was used to study mass transfer by crowdions initiated by the impact of a molecule on the end of the chain. It was shown that a molecule needs much less energy to initiate crowdions in the chain compared to a single atom.

In this work, the same model is used to analyze the modification of the crystal surface on molecule impact for different values of the impact velocity  $v_0$  and the number of atoms in the molecule  $N$ . We will focus on the analysis of the number of deposited or sputtered atoms. It will be shown that the formation of supersonic single and/or multiple crowdions plays a very important role in these processes. In particular, the nonmonotonic nature of the dependence of the sputtering yield on the molecular impact velocity  $v_0$  will be explained.

It is interesting to see what can be understood about the deposition and sputtering processes within the framework of the Frenkel-Kontorova model, perhaps the simplest one-dimensional model of a crystal.

In Sec. II we describe the Frenkel-Kontorova model and simulation setup. Phonons and subsonic crowdions are analyzed in Sec. III. Simulation results are presented in Sec. IV and analyzed in Sec. V. Conclusions are drawn in Sec. VI.

## II. MODEL AND SIMULATION SETUP

A chain of interacting particles placed in a sinusoidal on-site potential is called the Frenkel-Kontorova chain [53].

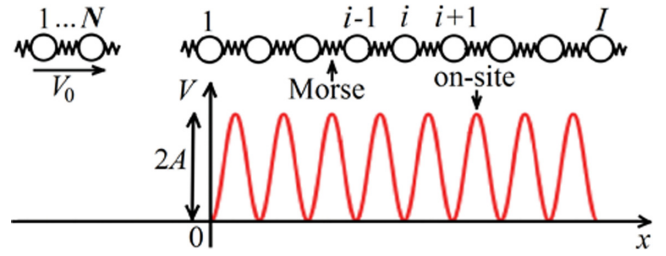


FIG. 1. Scheme of the simulation setup. Molecule of  $N$  atoms moves with the initial velocity  $v_0$  and hits the end of the Frenkel-Kontorova chain placed in sinusoidal on-site potential of depth  $2A$ . Each atom interacts with the nearest neighbors via the Morse potential. Atoms in the molecule are numbered with index  $n = 1, \dots, N$  and atoms in the chain with index  $i = 1, \dots, I$ . Total number of atoms in the system is  $N + I$ .

Consider a molecule of  $N$  atoms moving with the velocity  $v_0$  toward the left end of the chain, as shown in Fig. 1. Atoms in the molecule are numbered with index  $n = 1, \dots, N$  and atoms in the chain with index  $i = 1, \dots, I$ . Total number of atoms in the system is  $N + I$ . Hamiltonian of the molecule and chain system is given by

$$H = \sum_{n=1}^N \frac{m}{2} \left( \frac{dx_n}{dt} \right)^2 + \sum_{n=1}^{N-1} U(x_{n+1} - x_n) + \sum_{n=1}^N V(x_n) + \sum_{i=1}^I \frac{m}{2} \left( \frac{dx_i}{dt} \right)^2 + \sum_{i=1}^{I-1} U(x_{i+1} - x_i) + \sum_{i=1}^I V(x_i) + U(x_{i=1} - x_N), \quad (1)$$

where  $x_{n,i}(t)$  is the coordinate of the  $n, i$ -th atom. The terms in the right-hand side of Eq. (1) give the kinetic energy of atoms having mass  $m$ , the interaction energy of nearest neighbors via the potential  $U$ , and the energy of atoms in the on-site potential  $V$ . The last term describes the interaction of the first atom of the chain ( $i = 1$ ) with the  $N$ th atom of the molecule ( $n = N$ ).

The interatomic bonds are described by the Morse potential,

$$U(\xi) = D[1 + e^{-2\alpha(\xi - r_m)} - 2e^{-\alpha(\xi - r_m)}], \quad (2)$$

where  $D$  is the dissociation energy,  $r_m$  is the equilibrium interatomic distance, and  $\alpha$  defines the bond stiffness. We take  $D = 1$  and  $r_m = 1$ , which can be achieved by proper choice of the units of energy and distance. For the stiffness of the interatomic bond, we set the typical value  $\alpha = 4$ . The particle mass in our simulations is  $m = 1$ , which can always be achieved by choosing the unit of time.

The on-site potential is taken in the form

$$V(x) = \begin{cases} 0, & \text{for } x \leq 0, \\ A[1 - \cos(2\pi x)], & \text{for } x > 0. \end{cases} \quad (3)$$

This potential has an amplitude  $A$  and a period equal to 1, i.e., equal to the equilibrium interatomic distance  $r_m$ . The on-site potential is introduced to describe the interaction of the considered close-packed atomic row of the crystal lattice with the surrounding atoms. The potential acts only in the region  $x > 0$ , as shown in Fig. 1, since the crystal surface

is located at  $x = 0$ . Before the molecule reaches the end of the chain, it moves in vacuum without interacting with the on-site potential. The amplitude of the on-site potential is  $A = 2$ , which was justified in the work [47]. With this choice of  $A$ , the subsonic crowdion width is equal to half a dozen interatomic distances [see Fig. 2(b) in Sec. III B], which is a typical crowdion width in metals [41,42].

From the Hamiltonian defined by Eqs. (1)–(3) one can derive the following equations of motion for the atoms originally belonging to the molecule:

$$\begin{aligned}
 m\ddot{x}_n &= 2\alpha D[e^{-\alpha(x_{n+1}-x_n-r_m)} - e^{-2\alpha(x_{n+1}-x_n-r_m)} \\
 &\quad - H(x_n)2\pi A \sin(2\pi x_n), \quad \text{for } n = 1, \\
 m\ddot{x}_n &= 2\alpha D[e^{-\alpha(x_{n+1}-x_n-r_m)} - e^{-2\alpha(x_{n+1}-x_n-r_m)} \\
 &\quad + e^{-2\alpha(x_n-x_{n-1}-r_m)} - e^{-\alpha(x_n-x_{n-1}-r_m)}] \\
 &\quad - H(x_n)2\pi A \sin(2\pi x_n), \quad \text{for } n = 2, \dots, N-1, \\
 m\ddot{x}_n &= 2\alpha D[e^{-\alpha(x_{i=1}-x_n-r_m)} - e^{-2\alpha(x_{i=1}-x_n-r_m)} \\
 &\quad + e^{-2\alpha(x_n-x_{n-1}-r_m)} - e^{-\alpha(x_n-x_{n-1}-r_m)}] \\
 &\quad - H(x_n)2\pi A \sin(2\pi x_n), \quad \text{for } n = N,
 \end{aligned} \quad (4)$$

and similar equations for the atoms of the chain

$$\begin{aligned}
 m\ddot{x}_i &= 2\alpha D[e^{-\alpha(x_{i+1}-x_i-r_m)} - e^{-2\alpha(x_{i+1}-x_i-r_m)} \\
 &\quad + e^{-2\alpha(x_i-x_N-r_m)} - e^{-\alpha(x_i-x_N-r_m)}] \\
 &\quad - H(x_i)2\pi A \sin(2\pi x_i), \quad \text{for } i = 1, \\
 m\ddot{x}_i &= 2\alpha D[e^{-\alpha(x_{i+1}-x_i-r_m)} - e^{-2\alpha(x_{i+1}-x_i-r_m)} \\
 &\quad + e^{-2\alpha(x_i-x_{i-1}-r_m)} - e^{-\alpha(x_i-x_{i-1}-r_m)}] \\
 &\quad - H(x_i)2\pi A \sin(2\pi x_i), \quad \text{for } i = 2, \dots, I-1 \\
 m\ddot{x}_i &= e^{-2\alpha(x_i-x_{i-1}-r_m)} - e^{-\alpha(x_i-x_{i-1}-r_m)} \\
 &\quad - H(x_i)2\pi A \sin(2\pi x_i), \quad \text{for } i = I.
 \end{aligned} \quad (5)$$

In Eqs. (4) and (5)  $H(\eta)$  is the Heaviside function.

Note that the Hamilton Eq. (1) and the equations of motion (4) and (5) are written in a form that allows one to consider different atoms for the projectile and target. For this, it is necessary to use different parameters of the Morse potential Eq. (2) and different masses for the atoms of the molecule and the chain.

These equations of motion are integrated numerically using the Störmer symplectic method of the sixth order [54]. The time step was smaller for the higher impact velocity  $v_0$  and was chosen to achieve energy conservation with a relative error of no more than  $10^{-5}$  during the numerical experiment.

The initial coordinates of atoms are

$$\begin{aligned}
 x_n &= n - N - 5, \quad \text{for } n = 1, \dots, N, \\
 x_i &= i - 1, \quad \text{for } i = 1, \dots, I,
 \end{aligned} \quad (6)$$

and initial velocities of atoms are

$$\begin{aligned}
 \frac{dx_n}{dt} &= v_0, \quad \text{for } n = 1, \dots, N, \\
 \frac{dx_i}{dt} &= 0, \quad \text{for } i = 1, \dots, I.
 \end{aligned} \quad (7)$$

These initial conditions ensure that at  $t = 0$  the molecule practically does not interact with the chain because the distance between atoms  $N$  and  $i = 1$  is equal to 5, at which the Morse potential is negligibly small. The molecule moves toward the chain with the velocity  $v_0$ .

Initial energy of the molecule is

$$E_0 = \frac{Nmv_0^2}{2}. \quad (8)$$

We will consider molecules having the maximum number of atoms  $N = 4$  with the maximum speed  $v_0 = 50$ . This means that the maximum projectile energy in our simulations is  $E_0 = 5000$ . This energy is enough to break 5000 interatomic bonds, since in our calculations the bond energy is  $D = 1$ . Recall that in metals the evaporation energy is several eV per atom, and thus the evaporation of 5000 metal atoms will cost about 10 keV. This means that we are simulating a linear sputtering regime [12], when a relatively small number of defects are formed.

The sputtering yield  $Y$ , i.e., the average number of atoms removed from the target per one incident atom, is the most important characteristic of sputtering. It depends on the target material, on the species of bombarding atoms, on their energy and the angle of incidence [55,56]. Within the one-dimensional model, only normal incidence can be simulated.

Sputtered atoms are those that before the impact of the molecule belonged to the chain and after the impact have negative coordinates and negative velocities, moving (together with the  $N$  atoms of the molecule) away from the chain in vacuum. If the number of atoms with negative coordinates and negative velocities is equal to  $L$ , then the number of sputtered atoms is equal to  $L - N$  and the sputtering yield is defined as

$$Y = \frac{L - N}{N}. \quad (9)$$

### III. PHONONS AND CROWDIONS

A standard analysis of the properties of low-amplitude traveling waves and subsonic kinks is presented below.

#### A. Small-amplitude waves

Molecule with sufficiently large energy initiates moving crowdions (antikinks) in the chain. To distinguish between subsonic and supersonic crowdions we need to know the maximal group velocity of the small-amplitude phonon waves.

Linearization of Eq. (5) for the atoms far from the chain ends reads

$$m\ddot{u}_i = 2\alpha^2 D(u_{i-1} - 2u_i + u_{i+1}) - 4\pi^2 A u_i, \quad (10)$$

where  $u_i = x_i - i$  is the displacement of the atom from the lattice position. The solutions of Eq. (10) in the form of running phonon waves is  $u_n \sim \exp[\mathbf{i}(qn - \omega_q t)]$ , where  $\mathbf{i}$  is the imaginary unit,  $q$  is the wave number, and  $\omega_q$  is frequency. Substituting this form of the solution into Eq. (10) the following dispersion relation can be obtained:

$$\omega_q^2 = \frac{4}{m} [\pi^2 A - \alpha^2 D(\cos q - 1)]. \quad (11)$$

From Eq. (11) it follows that the chain supports the phonon waves with frequencies from  $\omega_{\min} = 2\pi\sqrt{A/m}$  to  $\omega_{\max} =$

$\sqrt{4\pi^2 A/m + 2\alpha^2 D}$ . Phonon's group velocity is defined by

$$v_g = \frac{d\omega_q}{dq} = \frac{\alpha^2 D \sin q}{m^2 \sqrt{\pi^2 A + \alpha^2 D(1 + \cos q)}}. \quad (12)$$

The group velocity vanishes for  $q \rightarrow 0$  and  $q \rightarrow \pm\pi$ . For the considered parameters of the chain this function has a maximum value of  $v_g^{\max} = 2.89$  at  $q = 1.33$ .

We conclude that the antikinks having speed below (above) 2.89 are subsonic (supersonic) antikinks.

### B. Subsonic antikink (crowdion)

Kink and antikink in the Frenkel-Kontorova model with harmonic interatomic potential have the same profile [53], but this is not the case for the asymmetric Morse potential. Stiffness of the Morse potential decreases (increases) under tension (compression) of the bond, while stiffness of the harmonic bond is strain independent.

For the harmonic interatomic interactions and in the long-wave approximation, the Frenkel-Kontorova chain can be approximated by the integrable sine-Gordon equation that supports kink solution [53]. First, in Eq. (5) for the atoms far from the chain ends we linearize the Morse interatomic interactions to obtain

$$m\ddot{u}_i = 2\alpha^2 D(u_{i-1} - 2u_i + u_{i+1}) - 2\pi A \sin(2\pi u_i), \quad (13)$$

where  $u_i = x_i - i$  is the displacement of the atom from the lattice position. This equation of motion can be rewritten in the form

$$\ddot{w}_i = \frac{1}{h^2}(w_{i-1} - 2w_i + w_{i+1}) - g^2 \sin(w_i), \quad (14)$$

where

$$w_i = 2\pi u_i, \quad h^2 = \frac{m}{2\alpha^2 D}, \quad g^2 = \frac{4\pi^2 A}{m}. \quad (15)$$

The sine-Gordon equation is obtained from Eq. (14) in the continuum limit,  $h \rightarrow 0$ :

$$w_{tt} - w_{xx} + g^2 \sin w = 0. \quad (16)$$

The antikink solution to Eq. (16) reads

$$w(x, t) = 2\pi - 4 \arctan \left[ \exp \left( g \frac{x - x_0 - vt}{\sqrt{1 - v^2}} \right) \right], \quad (17)$$

where  $v$  defines the antikink velocity and  $x_0$  is its initial position.

In terms of the original variable  $u_i$ , taking into account that  $x = ih$ , the approximate antikink solution to Eq. (13) has the form

$$u_i(t) = 1 - \frac{2}{\pi} \arctan \left\{ \exp \left[ g \frac{h(i - x_0) - vt}{\sqrt{1 - v^2}} \right] \right\}. \quad (18)$$

From this solution, kink velocity is equal to  $V_k = v/h$ . Since  $|v| < 1$ , the kink velocity is within the range

$$|V_k| < \frac{1}{h}. \quad (19)$$

Taking into account Eq. (15) we find that for parameters used in our study  $|V_k| < 5.66$ . When antikink speed approaches the

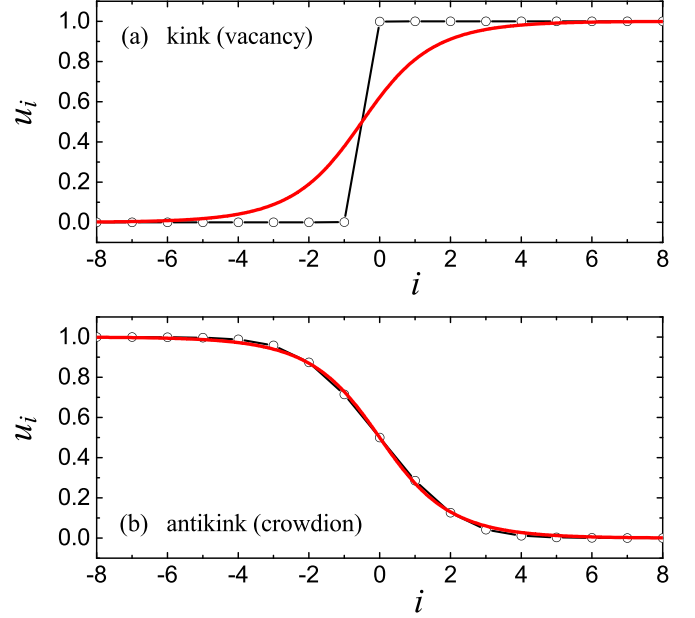


FIG. 2. (a) Numerical solution for the static kink, or vacancy (black symbols and line) compared to the analytical solution Eq. (18) with  $i \rightarrow -i$  (red line). (b) Numerical solution for the static antikink, or crowdion (black symbols and line), compared to the analytical solution Eq. (18) (red line).

maximal value, its width vanishes and the continuum approximation Eq. (16) cannot be used. We conclude that the antikink (crowdion) solution Eq. (18) can be used for velocities when the relativistic effects are small.

The numerically obtained solutions for static kink and antikink of the Frenkel-Kontorova model Eq. (4) are shown in Figs. 2(a) and 2(b), respectively, as black symbols and lines. The red lines show the symmetrical solution for kink and antikink, Eq. (18). It can be seen that the approximate solution for the antikink is quite good, but it cannot be used for the kink. Such a different profile of the kink and antikink is due to the asymmetry of the Morse potential. The solution (18) was obtained for the equation (13), which considers the linearized Morse potential. Replacing the Morse potential Eq. (2) with a square parabola works well for an antikink, which is a compressed region of the lattice and gives the wrong result for a kink, which is a stretched region of the lattice. The Morse potential becomes stiffer in compression and softer in tension and it actually breaks in the core of a kink. In materials science, such a sharp kink as in Fig. 2(a), with nearly broken interatomic bond, is called a vacancy, and an antikink in Fig. 2(b) is called a crowdion.

## IV. SIMULATION RESULTS

### A. Molecule-chain collision scenarios

We start presenting the numerical results by showing possible scenarios for the collision of molecules with the chain, see Fig. 3. Here coordinates of atoms originally belonging to the molecule,  $x_n$ , and of atoms of the chain near the chain end,  $x_i$ , are shown as the functions of time. Four columns of this figure present results for molecules with the number of atoms

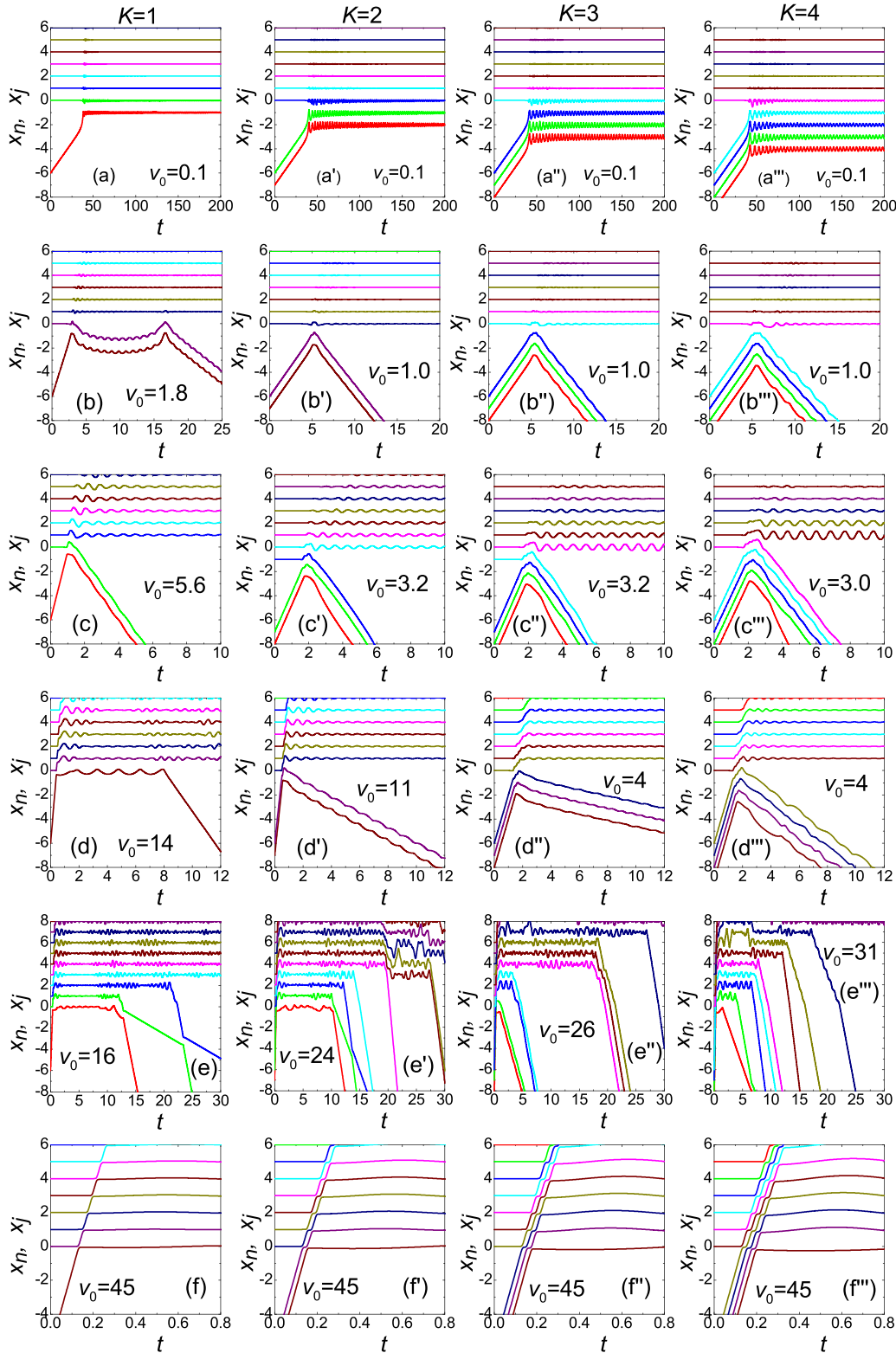


FIG. 3. Atomic coordinates as the functions of time, showing different scenarios of the molecule-chain collisions for a different number of atoms in the molecule  $N$  and for different initial velocities of the molecule  $v_0$ . Four columns correspond to bombardment by molecules having from  $N = 1$  to  $N = 4$  atoms. The initial velocity of the molecule  $v_0$  is given in each panel and it increases from top to bottom.

from  $N = 1$  to  $N = 4$ . The speed of the molecule increases from the top to the bottom of the figure.

In the first row of Figs. 3(a)–3(a'''), the collision velocity is low,  $v_0 = 0.1$ , and the molecules are deposited at

the end of the chain (on the crystal surface). Since the number of atoms moving away from the chain is  $L = 0$ , in these cases, the sputtering yield according to Eq. (9) is  $Y = -1$ .

In the second row of Fig. 3, the collision velocity is  $v_0 = 1.8$  in Fig. 3(b) and  $v_0 = 1.0$  for Figs. 3(b')–3(b''). In Figs. 3(b')–3(b'') the molecules are reflected from the chain almost elastically since the speed of the molecules after the collision is only slightly smaller than  $v_0$ . A small part of the energy  $E_0$  is given to excite vibrations in the chain and in the molecules. Sputtering yield in these cases is zero because  $L = N$ . The picture of collision is different in (b). Here the incident atom takes one atom from the chain and a biatomic molecule is reflected. In this case  $N = 1$ ,  $L = 2$  and Eq. (9) gives the sputtering yield  $Y = 1$ .

In the third row of Figs. 3(c)–3(c''), in all cases, the reflected molecule takes one atom from the chain and, consequently,  $Y = 1/N$ , because  $L = N + 1$ . Initial velocities of molecules are [Fig. 3(c)]  $v_0 = 5.6$ , [Fig. 3(c') and Fig. 3(c'')]  $v_0 = 3.2$ , and [Fig. 3(c'')]  $v_0 = 3.0$ . The energy of the molecule is spent to detach one atom from the chain and to excite vibrations in the chain and in the molecules.

It can be expected that a further increase in the initial velocity of the molecule will lead to an increase in the sputtering yield  $Y$ , but this is not the case in the fourth row of Figs. 3(d)–3(d''). Here  $v_0$  is greater than in Figs. 3(c)–3(c'') for any  $N$ , but the sputtering yield is  $Y = 0$ , since the molecules are reflected from the chain without carrying away the atoms. This result is explained by the fact that the incident molecules in Figs. 3(d)–3(d'') expend their energy to create a supersonic crowdion (antikink) that transfers energy deep into the chain. The energy of vibrations, which remains near the end of the chain, is not enough to break the interatomic bonds.

A further increase in the velocity of the molecule  $v_0$  leads to the creation of vacancies, subsonic and supersonic crowdions in the chain and an increase in the sputtering yield  $Y$ , see Figs. 3(e)–3(e''). It is noteworthy that the detachment of atoms from the chain does not occur instantly; atoms are detached from the chain one after another, and the sputtering process is extended in time. This is because the transfer of energy by phonons is rather slow. From Eq. (12) it was found that the maximum group velocity is  $v_g^{\max} = 2.89$  for  $q = 1.33$  and even less for phonons with the longer and shorter wavelengths. In Sec. IV C it will be shown that supersonic crowdions move at much higher speeds and carry large energy in a localized form, being much more efficient in energy transfer than phonons. In Figs. 3(e)–3(e'') supersonic crowdions were not formed and large-amplitude oscillations of atoms are visible, which occur due to the impact of molecules. With a certain probability, the energy of these oscillations is spent on the sputtering of atoms, and one by one they move away from the chain. The sputtering process slows down due to the fact that the energy of the chain is carried away by the sputtered atoms and also due to the slow transfer of energy deep into the chain by phonons.

The bottom row of Figs. 3(f)–3(f'') is built for the collision velocity  $v_0 = 45$ . It can be seen that supersonic  $N$ -crowdions are formed, which effectively transfer energy deep into the chain. Atomic vibrations of large amplitude, as in Figs. 3(e)–3(e''), are not visible. No atoms are removed from the chain ( $L = 0$ ) and thus  $Y = -1$  in all four cases. Note that in Figs. 3(a)–3(a''), the sputtering yield is also  $Y = -1$ , but the absorption of atoms in Figs. 3(f)–3(f'') is accompanied by

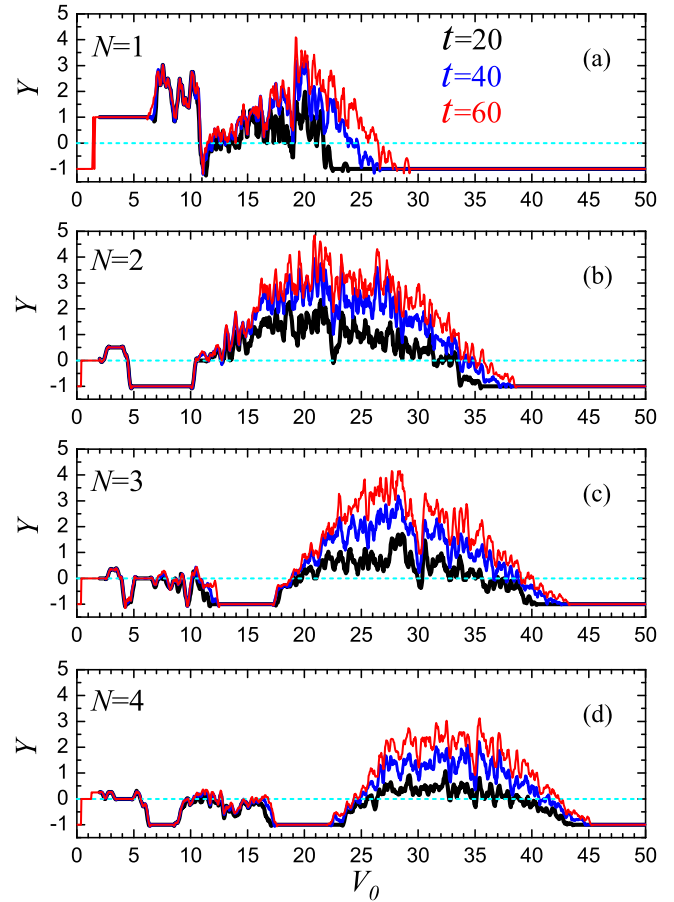


FIG. 4. The sputtering yield as the function of the velocity of the bombarding molecule for molecules with the number of atoms (a)–(d) from  $N = 1$  to 4, respectively. The sputtering yield is shown for  $t = 20$  (black),  $t = 40$  (blue), and  $t = 60$  (red). Sputtering is actually observed for  $Y > 0$ . When  $Y = 0$  the molecule is reflected from the chain. For  $Y < 0$  a part of the molecule (the whole molecule in the case of  $Y = -1$ ) is deposited in the chain.

the formation of supersonic  $N$ -crowdions, while in Figs. 3(a)–3(a'') crowdions are not formed.

It can be concluded that the sputtering yield  $Y$  has a nonmonotonic dependence on the initial velocity of the molecule  $v_0$ .

## B. Sputtering yield

Figure 4 shows how the sputtering yield depends on the collision velocity for the molecules with  $N$  atoms. In Figs. 4(a) to 4(d)  $N$  is equal to 1 to 4, respectively. To obtain the results shown in Fig. 4, the range of initial molecule velocity  $0 < v_0 \leq 50$  was scanned with the step of 0.05 and the sputtering yield was calculated with the use of Eq. (9) at  $t = 20$  (black lines),  $t = 40$  (blue lines), and  $t = 60$  (red lines). This presentation helps to see how the sputtering evolves in time. Note that numerical data was smoothed over 11 neighboring points using the Savitzky-Golay filter [57].

For small and large values of  $v_0$ , the sputtering yield does not change after  $t > 20$  but, as it was seen in Figs. 3(e)–3(e''), there is a window of  $v_0$ , where the detachment of atoms from the chain is extended in time.

The negative value of  $Y$  means that a part of the incident molecule (in the case of  $Y = -1$  the whole molecule) is deposited in the chain. Deposition of molecules, i.e.,  $Y = -1$ , is observed in several windows of the initial velocity of the molecule. At low collision velocities, the molecule sticks to the end of the chain, as in the first row of Fig. 3, and at high  $v_0$ , the molecule forms kinks that transfer the mass deep into the chain, as in the bottom row of Fig. 3.

When  $Y = 0$ , the molecule is reflected from the chain. At small  $v_0$  the reflection is nearly elastic, as in Figs. 3(b')–3(b''). At higher  $v_0$  the reflected molecule can initiate propagation of a supersonic kink in the chain, as in Figs. 3(d)–3(d''').

A positive  $Y$  means that the molecule is reflected and part of the chain is sputtered. The maximum of  $Y$  shifts toward higher molecule velocities with an increase in the number of atoms  $N$  in the molecule.

The sputtering yield depends nonmonotonically on the speed of the molecules, as already mentioned when discussing various scenarios of collision of molecules with the chain. An explanation will be given below.

### C. Supersonic crowdions

A molecule with a sufficiently high energy in the considered range of initial velocities  $v_0$  excites one or a few supersonic crowdions (antikinks) in the chain. Subsonic kink-antikink pairs are also formed, but first we will discuss the properties of supersonic antikinks. The velocity of supersonic crowdions,  $V_k$ , excited by a molecule with initial velocity  $v_0$  is presented in Fig. 5. Figures 5(a) to 5(d) show the results for molecules with  $N = 1$  up to 4 atoms, respectively. Six different types of supersonic crowdions were identified and are denoted by the Greek numerals. Only crowdions of type VI can have velocities within a certain range, while the other five types of crowdions propagate at the speed characteristic of this crowdion type.

Instant profiles of the five types of supersonic crowdions (from type I to type V) are plotted in Fig. 6. They emerged due to bombardment by the molecules with the parameters  $N = 1$ ,  $v_0 = 25$  (black circles);  $N = 1$ ,  $v_0 = 15$  (red squares);  $N = 2$ ,  $v_0 = 15$  (blue triangles);  $N = 3$ ,  $v_0 = 20$  (purple pentagons); and  $N = 4$ ,  $v_0 = 25$  (green rhombuses). Horizontal bars indicate the crowdion width. Crowdions I to III are single antikinks. Among them the widest is the crowdion of type I; its width is six lattice sites, with propagation velocity  $V_k = 5.7$  and energy  $E_k = 18.8$ . Crowdion II is narrower (five lattice sites); its propagation velocity is  $V_k = 8.1$  and energy  $E_k = 23.2$ . The narrowest single antikink III (four lattice sites) propagates at a speed  $V_k = 13.2$  and has energy  $E_k = 49.8$ . Double antikink IV has width of six lattice sites, propagation velocity  $V_k = 20.3$ , and energy  $E_k = 282$ . Triple antikink V has width of eight lattice sites, propagation velocity  $V_k = 25.6$ , and energy  $E_k = 734$ . Similar supersonic crowdions have been described by Savin with coworkers in Refs. [45,46] for the chain with cubic intersite and  $\phi^4$  on-site potentials. Their model also supports a finite number of supersonic antikink velocities at which they do not emit phonons. A nonradiating crowdion must have a width equal to an integer number of lattice steps, and its total amplitude must coincide with an integer number of on-site potential widths (see Fig. 6).

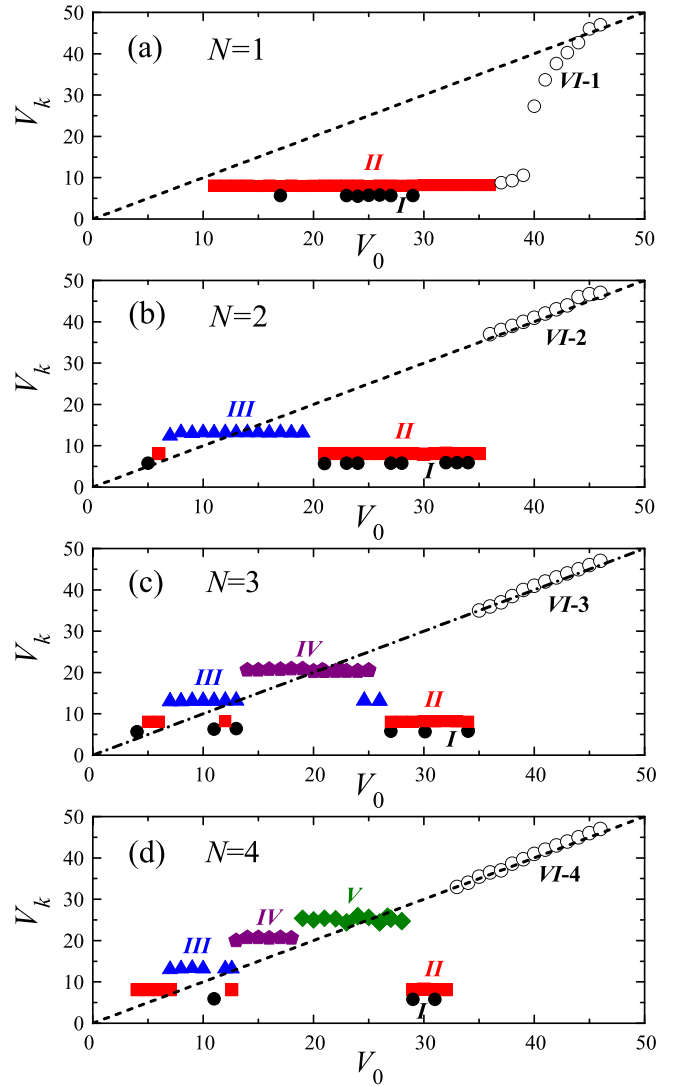


FIG. 5. Velocities of supersonic crowdions excited in the chain by the molecules with the velocity  $v_0$ . In (a) to (d) the number of atoms in the molecule  $N$  is equal to 1 to 4, respectively. Six types of supersonic crowdions were identified; they are numbered with Greek numerals (their profiles can be seen in Figs. 6 and 7). The dashed lines show the linear function  $V_k = v_0$ .

This explains why there are a finite number of propagation velocities for supersonic crowdions.

Supersonic crowdions of type VI can move at any speed within a certain range of speeds (see Fig. 5), which distinguishes them from supersonic crowdions of other types. Profiles of the crowdions of type VI are shown in Fig. 7 at  $t = 11$ . The multiple crowdions of type VI are unstable and relatively quickly split into single crowdions of type VI. The crowdions shown in Fig. 7 were obtained by bombardment with the molecules having velocity  $v_0 = 45$  and number of atoms from  $N = 1$  to  $N = 4$ , they are designated as VI-1 to VI-4, respectively. The distance between subkinks increases with time.

Steady motion of supersonic crowdions of types I to VI can be seen in Figs. 8–13, respectively. Time evolution of (a) displacements and (b) energies of four neighboring particles

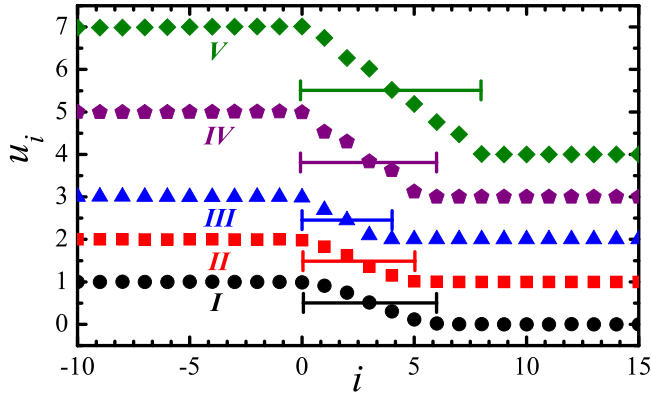


FIG. 6. Profiles of the supersonic crowdions. From bottom to top: 1-crowdion I with  $V_k = 5.7$ , 1-crowdion II with  $V_k = 8.1$ , 1-crowdion III with  $V_k = 13.2$ , 2-crowdion IV with  $V_k = 20.3$ , and 3-crowdion V with  $V_k = 25.6$ . The horizontal bars show the width of the crowdion.

are shown during passing of crowdions. It can be seen that passing single crowdions shift the particles by one lattice site [Figs. 8(a), 9(a), 10(a), and 13(a)], while double- and triple-crowdions shift the particles by two and three lattice sites, respectively; see Figs. 11(a) and 12(a). The crowdions propagate radiating energy very slowly, so that the energies of the particles after passing of the kink are practically zero, see panels (b) in Figs. 8–13.

An analysis of the dynamics of crowdions helps to understand why the velocity of crowdions of type VI can vary in a certain range of velocities. Crowdions of type VI have highest speed and highest energy compared to the crowdions of other types. In crowdion of type VI only one atom moves at a high speed, as can be seen in Fig. 13(a). Transmission of energy

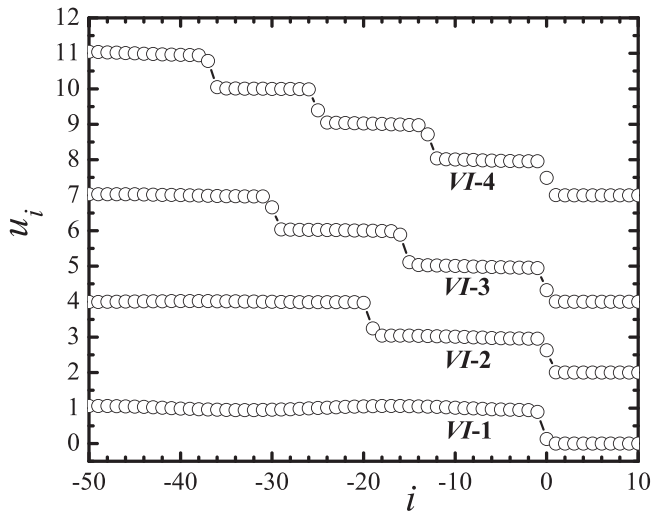


FIG. 7. Profiles of supersonic crowdions of type VI at  $t = 11$ . The crowdions are obtained by bombarding with molecules with a speed of  $v_0 = 45$  and the number of atoms from  $N = 1$  to  $N = 4$ ; they are designated as VI-1 to VI-4, respectively. All crowdions move at a speed of  $V_k \approx 46$ . Having just formed, they look like multiple crowdions, but after a short time they split into single crowdions of type VI, and the distance between them increases with time.

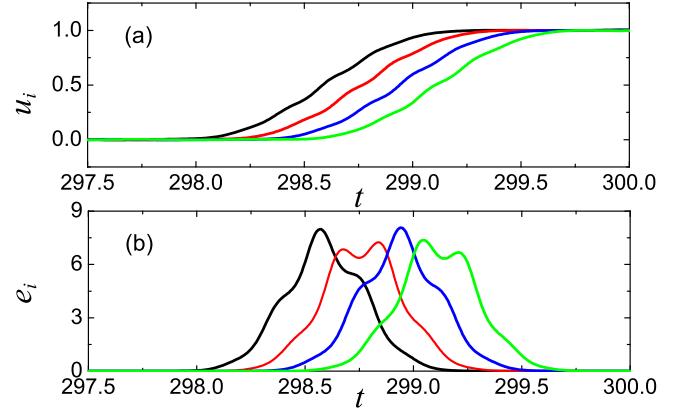


FIG. 8. Motion of a supersonic single-crowdion of type I launched with the atom ( $N = 1$ ) having initial velocity  $v_0 = 15$ . The crowdion velocity is  $V_k = 5.7$  and energy  $E_k = 18.8$ . As the functions of time shown are (a) displacements of the four nearest particles and (b) energies of the same four particles.

between colliding atoms takes place within single well of the on-site potential. As shown in Refs. [45,46], there exist a finite number of supersonic antikink velocities at which they do not emit phonons, and they correspond to bound states of acoustic solitons whose total amplitude coincides with the width of the on-site potential. At very high crowdion energies, the on-site potential does not play a significant role.

Time evolution of the energy of supersonic crowdions is shown in Fig. 14. Figures 14(a) to 14(c) show the results for single crowdions of the I, II, and III types, respectively. Figure 14(d) is for double crowdion IV, Fig. 14(e) for triple crowdion V, and Fig. 14(f) for single crowdion VI. The crowdions are formed as a result of the collision of molecules with the chain and initially they carry some perturbations. As they move deeper into the chain, the crowdions take on stationary profiles, shown in Figs. 6 and 7. In the regime of stationary motion, the crowdions I to V practically do not radiate energy. Less stable among them is the triple crowdion of type V, which

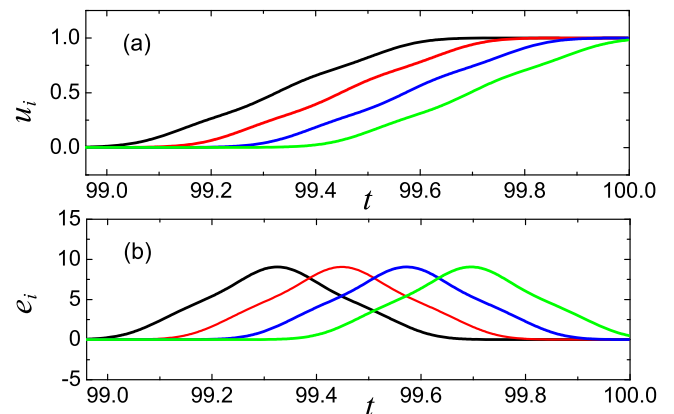


FIG. 9. Motion of a supersonic single-crowdion of type II launched with the atom ( $N = 1$ ) having initial velocity  $v_0 = 15$ . The crowdion velocity is  $V_k = 8.1$  and energy  $E_k = 23.2$ . As the functions of time shown are (a) displacements of the four nearest particles and (b) energies of the same four particles.

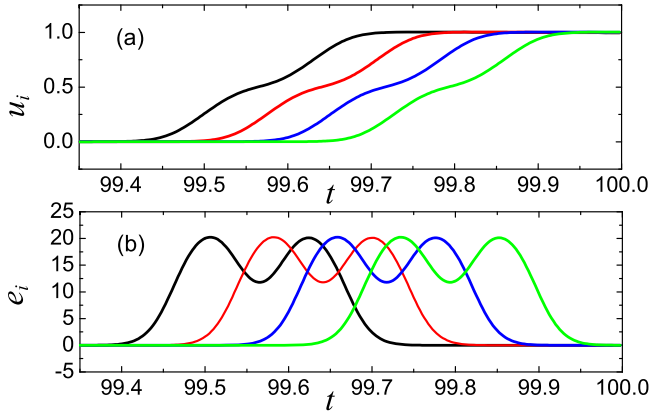


FIG. 10. Motion of a supersonic single-crowdion of type III launched with the  $N = 2$  molecule with the initial velocity  $v_0 = 15$ . The crowdion velocity is  $V_k = 13.2$  and energy  $E_k = 49.8$ . As the functions of time shown are (a) displacements of the four nearest particles and (b) energies of the same four particles.

at  $t = 410$  decays into single crowdion of type III and double crowdion of type IV. But before splitting, it travels a distance exceeding  $10^4$  lattice sites. Supersonic crowdions from I to IV showed no signs of degradation at time  $t = 800$ . Crowdion VI slowly radiates energy in the form of small-amplitude phonon waves, as can be seen in Fig. 14(f). The radiation rate increases with decreasing crowdion velocity.

The plateau values of the energies of supersonic crowdions,  $E_k$ , and the velocities of their steady motion,  $V_k$ , are displayed in Table I.

## V. DISCUSSION OF THE RESULTS

The numerical results presented in the Sec. IV are discussed below.

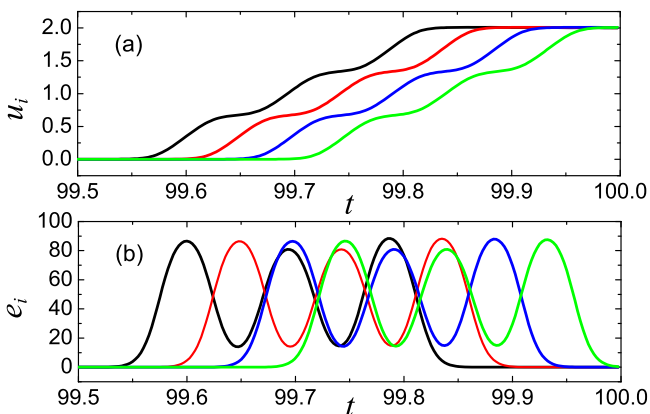


FIG. 11. Motion of a supersonic double-crowdion of type IV launched with the  $N = 3$  molecule with the initial velocity  $v_0 = 20$ . Crowdion velocity is  $V_k = 20.3$  and energy  $E_k = 282$ . As the functions of time shown are (a) displacements of the four nearest particles and (b) energies of the same four particles.

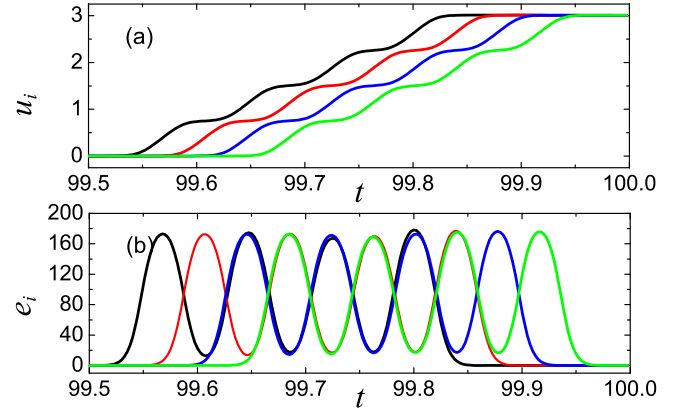


FIG. 12. Motion of a supersonic triple-crowdion of type V launched with the  $N = 4$  molecule with the initial velocity  $v_0 = 25$ . Crowdion velocity is  $V_k = 25.6$  and energy  $E_k = 734$ . As the functions of time shown are (a) displacements of the four nearest particles and (b) energies of the same four particles.

### A. Relation between sputtering yield and generation of supersonic crowdions

The sputtering yield is high when the energy transferred to the chain from the bombarding molecule does not penetrate deep into the chain but remains near the end of the chain (i.e., at the crystal surface). In this case, many vacancies and subsonic crowdions are formed near the end of the chain. The movement of these defects leads to the detachment of atoms from the end of the chain one by one, as shown in Figs. 3(e)–3(e''').

To illustrate the above, let us dwell on the discussion of the sputtering yield caused by a molecule of  $N = 3$  atoms shown in Fig. 4(c). It is interesting to analyze the energy flow in the system for the molecule initial velocities  $v_0 = 15, 26$ , and  $45$ . At  $v_0 = 26$  the sputtering yield is high, and in two other cases the molecule is deposited on the chain and  $Y = -1$ .

For the case of  $N = 3$  and  $v_0 = 15$ , in Fig. 15(a) we plot displacements of particles and in Fig. 15(b) energies of parti-

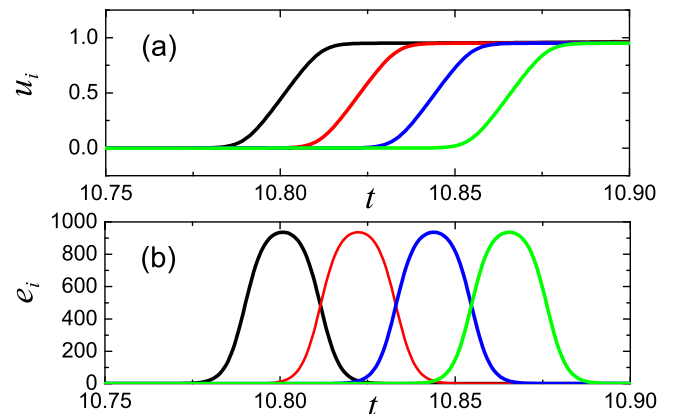


FIG. 13. Motion of a supersonic single-crowdion of type VI launched with the  $N = 1$  molecule with the initial velocity  $v_0 = 45$ . Crowdion velocity is  $V_k = 46.5$  and energy  $E_k = 966$  (at  $t = 10$ ). As the functions of time shown are (a) displacements of the four nearest particles and (b) energies of the same four particles.

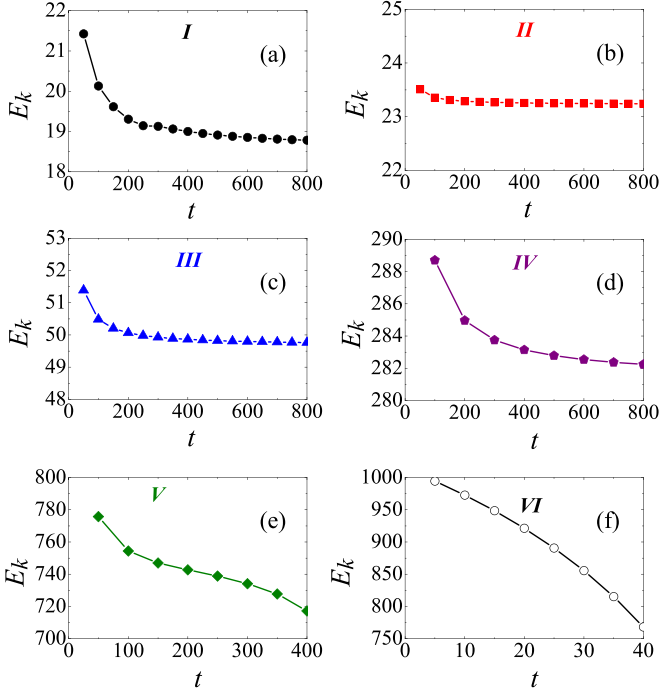


FIG. 14. Energy of the supersonic crowdions as the functions of time. (a) Single crowdion of type I, (b) single crowdion of type II, (c) single crowdion of type III, (d) double crowdion of type IV, (e) triple crowdion of type V, and (f) single crowdion of type VI.

cles at  $t = 5$ . Propagation of the supersonic double crowdion of type VI bearing an internal vibrational mode can be seen. The crowdion radiates energy in the form of small-amplitude phonons. At  $t = 5$  the crowdion has energy  $E_k = 324.7$ . The energy radiated by the crowdion at  $t = 5$  is  $E_r = 12.8$ . The sum of these energies is equal to the initial energy of the molecule  $E_k + E_r = E_0 = 337.5$ . This means that there is no energy in the system to break interatomic bonds to sputter atoms and hence  $Y = -1$ .

In Fig. 16, similar results are presented for  $N = 3$  and  $v_0 = 45$ . The supersonic triple crowdion of type VI-3 is formed, see also Fig. 3(f''). The crowdion at  $t = 2$  has energy  $E_k = 2984.3$ . The energy radiated by the crowdion at  $t = 2$  is  $E_r = 53.2$ . The sum of these energies is equal to the initial energy of the molecule  $E_k + E_r = E_0 = 3037.5$ . There is no energy in the system to break interatomic bonds and thus  $Y = -1$ .

A qualitatively different picture is observed in the case  $N = 3$  and  $v_0 = 26$ , see Fig. 17. In this case the sputtering yield is

TABLE I. Speed and energy of the supersonic crowdions in the regime of stationary motion.

Crowdion type	speed, $V_k$	energy, $E_k$
I, single	5.7	18.8
II, single	8.1	23.2
III, single	13.2	49.8
IV, double	20.3	282
V, triple	25.6	734
VI-1, single	46.5	966

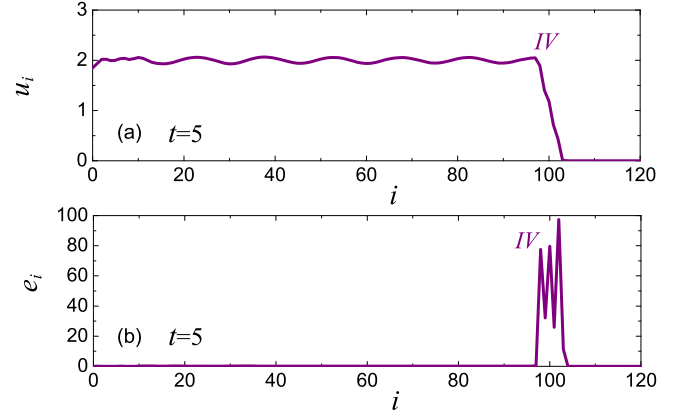


FIG. 15. Distribution of (a) atom displacements and (b) atom energies over the chain at  $t = 5$  after bombardment with the molecule of  $N = 3$  atoms with the initial velocity  $v_0 = 15$ . A supersonic double crowdion of type IV is formed. The molecule is deposited on the chain, sputtering is not observed.

positive, see also Fig. 3(e''). Two supersonic kinks of type I and type II are formed with total energy  $E_{kI} + E_{kII} = 42$ . The energy transferred to the system by the molecule is equal to  $E_0 = 1014$ . It can be seen that most of this energy remains near the chain end. A series of subsonic kinks and vacancies is created, which leads to the sputtering of atoms.

## B. Comparison to existing data

The main result of this study is shown in Fig. 4, where the sputtering yield as the function of the molecule velocity is plotted for a different number of atoms in the bombarding molecule. Bombardment with small velocity ( $v_0$  up to 1.5 for  $N = 1$  and up to 0.3 for  $N > 1$ ) results in deposition of molecules without structural changes in the chain, similarly to what is observed experimentally [11,15]. In our simulations, deposition of molecule accompanied by formation of supersonic crowdions transferring interstitials deep into the chain

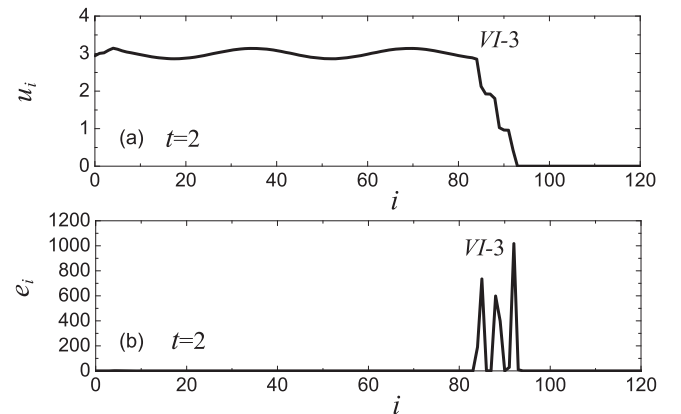


FIG. 16. Distribution of (a) atom displacements and (b) atom energies over the chain at  $t = 2$  after bombardment with the molecule of  $N = 3$  atoms with the initial velocity  $v_0 = 45$ . A supersonic triple crowdion of type VI-3 is formed. The molecule is deposited on the chain, sputtering is not observed.

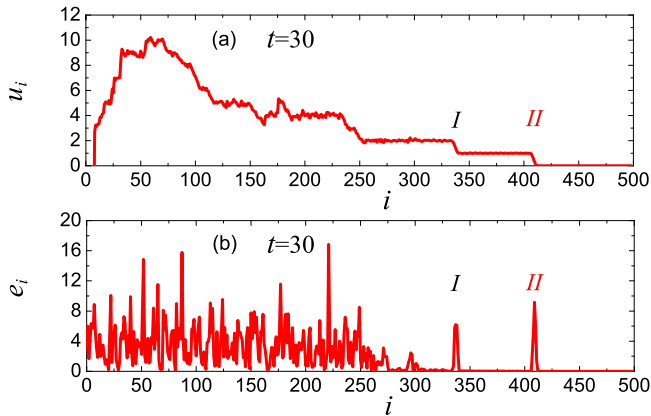


FIG. 17. Distribution of (a) atom displacements and (b) atom energies over the chain at  $t = 30$  after bombardment with the molecule of  $N = 3$  atoms with the initial velocity  $v_0 = 26$ . Two supersonic single crowdions of types I and II are formed. The impact of the molecules caused sputtering.

is observed in the range  $5 < v_0 < 10$  for  $N = 2$ ,  $12.5 < v_0 < 17.5$  for  $N = 3$ , and  $17 < v_0 < 22$  for  $N = 4$ .

The regime of sputtering in Fig. 4 is observed in the range of molecule velocity  $11 < v_0 < 30$  for  $N = 1$ ,  $11 < v_0 < 38$  for  $N = 2$ ,  $18 < v_0 < 43$  for  $N = 3$ , and  $22 < v_0 < 45$  for  $N = 4$ . The sputtering yield is maximal when  $v_0 = 20$ ,  $E_0 = 200$  for  $N = 1$ ;  $v_0 = 23$ ,  $E_0 = 529$  for  $N = 2$ ,  $v_0 = 28$ ,  $E_0 = 1176$  for  $N = 3$ , and  $v_0 = 33$ ,  $E_0 = 2178$  for  $N = 4$ . At higher molecular energies, the sputtering yield decreases monotonically, and eventually the molecules are deposited to the chain with the formation of supersonic  $N$ -crowdions of type VI. It is also observed in experiments that at very high ion energies (above 50 keV), the overall sputtering yield decreases due to deep implantation of ions into the target [5]. In this regard, the simulation data obtained for the simple Frenkel-Kontorova model are in fairly good qualitative agreement with experimental observations.

Recall that the binding energy in the Frenkel-Kontorova chain under consideration is equal to  $D = 1$ , and the heat of vaporization for metals is about 300 kJ/mol, i.e., about 3 eV per atom. This means that the units of energy used in our simulations can be converted to eV by multiplying by a factor of 3. The maximum sputtering yield found for the Frenkel-Kontorova model lies in the range  $200 < E_0 < 2000$  for various  $N$ , which corresponds to the energy range from 600 eV to 6 keV for metals. This agrees with the experimental data, according to which the maximum sputtering coefficient is observed for ions with energy between 1 and 10 keV [18,19].

As shown in Fig. 5, the bombardment of the chain by molecules with sufficiently high energy leads to the formation of supersonic crowdions, their stationary profiles are plotted in Figs. 6 and 7. Crowdions of types I to V can propagate at a certain speed, and the highest energy crowdions of type VI can have a speed in a certain range. Previously similar crowdions, except for type VI, were described in the  $\phi^4$  chain with the Toda interparticle potential [45,46]. Isolated values of kink

velocity for which radiationless kink propagation is possible have been reported for the exceptional discretizations of the  $\phi^4$  model [58,59].

In the one-dimensional Frenkel-Kontorova model, atoms have one degree of freedom and are forced to move only along the chain. In three-dimensional crystals, atoms in a close-packed atomic row have lateral degrees of freedom and the problem of self-focusing atomic collisions becomes important [60]. Very fast collisions lead to a decrease in the effective diameter of atoms, and the collisions become defocusing [51]. This means that the very fast supersonic crowdions described in this work may be unstable in three-dimensional crystals.

In the works [23,24] sputtering yield was calculated using molecular dynamics and Lennard-Jones potentials for bcc and fcc crystals with (001) surface. In these cases, close-packed directions are not parallel to the ion beam, and the formation of crowdions is difficult. Nevertheless, the results of the present work, in which bombardment along a close-packed direction was simulated, are in qualitative agreement with these works.

## VI. CONCLUSIONS

In this work, the impact of molecules with  $N = 1$  up to 4 atoms on the free end of the Frenkel-Kontorova chain introduced in Ref. [47] was simulated. Depending on the collision velocity  $v_0$  various collision scenarios were described, see Fig. 3. The two main outcomes of the collision are the deposition of molecules and the sputtering of atoms from the chain. It was found that sputtering was observed in a window of collision velocities for any  $N$ . Formation of supersonic crowdions (antikinks) propagating along the chain explains this effect. At moderate values of  $v_0$  supersonic crowdions of types I to V are formed (see Fig. 5), they can propagate without radiating phonon waves only at particular speed, specific for each crowdion type (this fact has been established earlier for the  $\phi^4$  model in the works [45,46] and for the model considered here in Ref. [47]). At high impact velocities, supersonic crowdions of type VI are formed, which can have a speed in a certain range. When supersonic crowdions carry the impact energy deep into the chain, the sputtering is minimal and increases when the energy is transported by slowly moving phonons and remains near the end of the chain for a relatively long time.

Analysis of the existing experimental and theoretical works on atomic deposition and sputtering in Sec. VB showed that the obtained numerical results are in qualitative agreement with the available data.

## ACKNOWLEDGMENTS

D.U.A. is grateful for financial support to the Ministry of Science and Higher Education of the Russian Federation within the framework of the state task of the USATU (No. 075-03-2022-318/1) of the youth research laboratory Metals and Alloys under Extreme Impacts. For M.V.Kh. and Yu.V.B. this work was supported by the Russian Science Foundation, Grant No. 22-22-00810. S.V.D. acknowledges the support of Grant No. NSh-4320.2022.1.2 of the President of the Russian Federation for state support of young Russian scientists-candidates of sciences and doctors of sciences.

- [1] T. Som and D. Kanjilal, *Nanofabrication by Ion-Beam Sputtering: Fundamentals and Applications* (CRC, Taylor & Francis Group, London, 2012).
- [2] Edited by N. Yao, *Focused Ion Beam Systems, Basics and Applications* (Cambridge University Press, Cambridge, 2007).
- [3] M. Lang, F. Zhang, J. Zhang, J. Wang, B. Schuster, C. Trautmann, R. Neumann, U. Becker, and R. C. Ewing, Nanoscale manipulation of the properties of solids at high pressure with relativistic heavy ions, *Nat. Mater.* **8**, 793 (2009).
- [4] O. Ochedowski, O. Osmani, M. Schade, B. K. Bussmann, B. Ban-d'Etat, H. Lebius, and M. Schleberger, Graphitic nanostripes in silicon carbide surfaces created by swift heavy ion irradiation, *Nat. Commun.* **5**, 3913 (2014).
- [5] K. Nordlund, J. Keinonen, M. Ghaly, and R. S. Averback, Coherent displacement of atoms during ion irradiation, *Nature (Lond.)* **398**, 49 (1999).
- [6] B. P. Uberuaga, M. Tang, C. Jiang, J. A. Valdez, R. Smith, Y. Wang, and K. E. Sickafus, Opposite correlations between cation disordering and amorphization resistance in spinels versus pyrochlores, *Nat. Commun.* **6**, 8750 (2015).
- [7] Y. Zhang, A. Debelle, A. Boulle, P. Kluth, and F. Tuomisto, Advanced techniques for characterization of ion beam modified materials, *Curr. Opin. Solid State Mater. Sci.* **19**, 19 (2015).
- [8] M. Nastasi and J. W. Mayer, *Ion Implantation and Synthesis of Materials* (Springer, Berlin, 2006).
- [9] H.-C. Huang, J. I. Dadap, G. Malladi, I. Kymissis, H. Bakhru, and R. M. Osgood, Helium-ion-induced radiation damage in LiNbO<sub>3</sub> thin-film electro-optic modulators, *Opt. Express* **22**, 19653 (2014).
- [10] T. Ozaki, L. Wu, C. Zhang, J. Jaroszynski, W. Si, J. Zhou, Y. Zhu, and Q. Li, A route for a strong increase of critical current in nanostrained iron-based superconductors, *Nat. Commun.* **7**, 13036 (2016).
- [11] P. Sigmund, Six decades of atomic collisions in solids, *Nucl. Instrum. Methods B* **406**, 391 (2017).
- [12] P. Sigmund, Mechanisms and theory of physical sputtering by particle impact, *Nucl. Instrum. Methods B* **27**, 1 (1987).
- [13] M. Kaur, S. Gautam, and N. Goyal, Ion-implantation and photovoltaics efficiency: A review, *Mater. Lett.* **309**, 131356 (2022).
- [14] A. Debelle, J.-P. Crocombette, A. Boulle, A. Chartier, T. Jourdan, S. R. M. Pellegrino, D. Bachiller-Perea, D. Carpentier, J. Channagiri, T. H. Nguyen, F. Garrido, and L. Thomé, Lattice strain in irradiated materials unveils a prevalent defect evolution mechanism, *Phys. Rev. Materials* **2**, 013604 (2018).
- [15] P. M. Martin, Deposition technologies: An overview, in *Handbook of Deposition Technologies for Films and Coatings*, 3rd ed., edited P. M. Martin (Elsevier Inc., Burlington, MA, 2010), pp. 1–30.
- [16] J. Roth, W. Eckstein, and M. Guseva, Erosion of Be as plasma-facing material, *Fusion Eng. Des.* **37**, 465 (1997).
- [17] G. De Temmerman, K. Heinola, D. Borodin, S. Brezinsek, R. P. Doerner, M. Rubel, E. Fortuna-Zalesna, C. Linsmeier, D. Nishijima, K. Nordlund, M. Probst, J. Romazanov, E. Safi, T. Schwarz-Selinger, A. Widdowson, B. J. Braams, H.-K. Chung, and C. Hill, Data on erosion and hydrogen fuel retention in Beryllium plasma-facing materials, *Nucl. Mater. Energy* **27**, 100994 (2021).
- [18] M. I. Guseva, V. M. Gureev, S. N. Korshunov, V. E. Neumoin, Yu. A. Sokolov, V. G. Stolyarova, V. I. Vasiliev, S. V. Rylov, and V. M. Strunnikov, Self-sputtering of beryllium and sputtering and erosion of C-C composite in the experiments on plasma disruption simulation, *J. Nucl. Mater.* **220-222**, 957 (1995).
- [19] Y. Yamamura and H. Tawara, Energy dependence of ion-induced sputtering yields from monatomic solids at normal incidence, *At. Data Nucl. Data Tables* **62**, 149 (1996).
- [20] G. A. Bleykher, A. V. Yuryeva, A. S. Shabunin, V. P. Krivobokov, and D. V. Sidelev, The role of thermal processes and target evaporation in formation of self-sputtering mode for copper magnetron sputtering, *Vacuum* **152**, 156 (2018).
- [21] J. Fu, P. Ding, F. Dorleans, Z. Xu, and F. Chen, Deposition of copper by using self-sputtering, *J. Vac. Sci. Technol. A* **17**, 2830 (1999).
- [22] Z. J. Radzimski, W. M. Posadowski, S. M. Rosnagel, and S. Shingubara, Directional copper deposition using dc magnetron self-sputtering, *J. Vac. Sci. Technol. B* **16**, 1102 (1998).
- [23] N. A. Mauchamp and S. Hamaguchi, Why are physical sputtering yields similar for incident ions with different masses? Physical sputtering yields of the Lennard-Jones system, *J. Phys. D: Appl. Phys.* **55**, 225209 (2022).
- [24] N. A. Mauchamp, K. Ikuse, M. Isobe, and S. Hamaguchi, Self-sputtering of the Lennard-Jones crystal, *Phys. Plasmas* **29**, 023507 (2022).
- [25] B. J. Murdoch, A. J. Barlow, I. W. Fletcher, and P. J. Cumpson, The plasmonic properties of argon cluster-bombarded InP surfaces, *Appl. Phys. Lett.* **111**, 081603 (2017).
- [26] P. J. Cumpson, N. Sano, A. J. Barlow, and J. F. Portoles, Stability of reference masses: VII. cleaning methods in air and vacuum applied to a platinum mass standard similar to the international and national kilogram prototypes, *Metrologia* **50**, 532 (2013).
- [27] A. Delcorte, O. A. Restrepo, K. Hamraoui, and B. Czerwinski, Cluster impacts in organics: Microscopic models and universal sputtering curves, *Surf. Interface Anal.* **46**, 46 (2014).
- [28] D. Maciazek, R. J. Paruch, Z. Postawa, and B. J. Garrison, Micro- and macroscopic modeling of sputter depth profiling, *J. Phys. Chem. C* **120**, 25473 (2016).
- [29] R. J. Paruch, Z. Postawa, and B. J. Garrison, Physical basis of energy per cluster atom in the universal concept of sputtering, *J. Vac. Sci. Technol. B* **34**, 03H105 (2016).
- [30] P. J. Cumpson, M. Jaskiewicz, and W. K. Kim, Argon cluster-ion sputter yield: Molecular dynamics simulations on silicon and equation for estimating total sputter yield, *Surf. Interface Anal.* **54**, 341 (2022).
- [31] D. R. Mason, A. E. Sand, X. Yi, and S. L. Dudarev, Direct observation of the spatial distribution of primary cascade damage in tungsten, *Acta Mater.* **144**, 905 (2018).
- [32] J. Wang, Q. Hou, and B. L. Zhang, Migration behavior of self-interstitial defects in tungsten and iron, *Solid State Commun.* **325**, 114158 (2021).
- [33] J. Wang, B. He, W. Song, and W. Dang, Energetics, kinetics and dynamics of self-interstitial clusters in bcc tungsten, *Mol. Simul.* **45**, 666 (2019).
- [34] J. Fang, L. Liu, N. Gao, W. Hu, and H. Deng, Molecular dynamics simulation of the behavior of typical radiation defects under stress gradient field in tungsten, *J. Appl. Phys.* **130**, 125103 (2021).
- [35] A. Chartier and M.-C. Marinica, Rearrangement of interstitial defects in alpha-Fe under extreme condition, *Acta Mater.* **180**, 141 (2019).

- [36] F. Cheng, Q. Zheng, Y. Li, C. Zhang, and Z. Zeng, Electronic energy loss assessment in theoretical modeling of primary radiation damage in tungsten, *Int. J. Mod. Phys. C* **32**, 2150134 (2021).
- [37] N. Castin, A. Bakaev, G. Bonny, A. E. Sand, L. Malerba, and D. Terentyev, On the onset of void swelling in pure tungsten under neutron irradiation: An object kinetic Monte Carlo approach, *J. Nucl. Mater.* **493**, 280 (2017).
- [38] P. M. Derlet, D. Nguyen-Manh, and S. L. Dudarev, Multiscale modeling of crowdion and vacancy defects in body-centered-cubic transition metals, *Phys. Rev. B* **76**, 054107 (2007).
- [39] P.-W. Ma, D. R. Mason, and S. L. Dudarev, Multiscale analysis of dislocation loops and voids in tungsten, *Phys. Rev. Materials* **4**, 103609 (2020).
- [40] S. L. Dudarev, D. R. Mason, E. Tarleton, P.-W. Ma, and A. E. Sand, A multi-scale model for stresses, strains and swelling of reactor components under irradiation, *Nucl. Fusion* **58**, 126002 (2018).
- [41] S. L. Dudarev and P.-W. Ma, Elastic fields, dipole tensors, and interaction between self-interstitial atom defects in bcc transition metals, *Phys. Rev. Materials* **2**, 033602 (2018).
- [42] E. A. Korznikova, V. V. Shunaev, I. A. Shepelev, O. E. Glukhova, and S. V. Dmitriev, Ab initio study of the propagation of a supersonic 2-crowdion in fcc Al, *Comput. Mater. Sci.* **204**, 111125 (2022).
- [43] V. D. Natsik and S. N. Smirnov, Dislocations and crowdions in two-dimensional crystals. Part III: Plastic deformation of the crystal as a result of defect movement and defect interaction with the field of elastic stresses, *Low Temp. Phys.* **42**, 207 (2016).
- [44] S. A. Starikov, A. R. Kuznetsov, and V. V. Sagaradze, Crowdion in deformed fcc metal. Atomistic Modeling, *Phys. Met. Metallogr.* **122**, 1207 (2021).
- [45] A. V. Savin, Supersonic regimes of motion of a topological soliton, *J. Exp. Theor. Phys.* **81**, 608 (1995).
- [46] Y. Zolotaryuk, J. C. Eilbeck, and A. V. Savin, Bound states of lattice solitons and their bifurcations, *Physica D* **108**, 81 (1997).
- [47] A. Moradi Marjaneh, D. Saadatmand, I. Evazzade, R. Babicheva, E. Soboleva, S. Narasimalu, K. Zhou, E. Korznikova, and S. Dmitriev, Mass transfer in the Frenkel-Kontorova chain initiated by molecule impact, *Phys. Rev. E* **98**, 023003 (2018).
- [48] S. V. Dmitriev, E. A. Korznikova, and A. P. Chetverikov, Supersonic N-crowdions in a two-dimensional Morse crystal, *J. Exp. Theor. Phys.* **126**, 347 (2018).
- [49] I. A. Shepelev, E. A. Korznikova, D. V. Bachurin, A. S. Semenov, A. P. Chetverikov, and S. V. Dmitriev, Supersonic crowdion clusters in 2D Morse lattice, *Phys. Lett. A* **384**, 126032 (2020).
- [50] I. A. Shepelev, D. V. Bachurin, E. A. Korznikova, and S. V. Dmitriev, Highly efficient energy and mass transfer in bcc metals by supersonic 2-crowdions, *J. Nucl. Mater.* **568**, 153841 (2022).
- [51] S. V. Dmitriev, N. N. Medvedev, A. P. Chetverikov, K. Zhou, and M. G. Velarde, Highly enhanced transport by supersonic N-crowdions, *Phys. Status Solidi RRL* **11**, 1700298 (2017).
- [52] R. I. Babicheva, I. Evazzade, E. A. Korznikova, I. A. Shepelev, K. Zhou, and S. V. Dmitriev, Low-energy channel for mass transfer in Pt crystal initiated by molecule impact, *Comput. Mater. Sci.* **163**, 248 (2019).
- [53] O. M. Braun and Y. S. Kivshar, *The Frenkel-Kontorova Model: Concepts, Methods, and Applications* (Springer-Verlag, Berlin, 2004).
- [54] N. S. Bakhvalov, *Numerical Methods: Analysis, Algebra, Ordinary Differential Equations* (MIR Publishers, Moscow, 1977).
- [55] S. Shermukhamedov, L. Chen, R. Nazmutdinov, A. Kaiser, and M. Probst, Modelling the sputtering and reflection from a beryllium surface: Atomistic analysis, *Nucl. Fusion* **61**, 086013 (2021).
- [56] S. Shermukhamedov, L. Chen, R. Nazmutdinov, and M. Probst, Sputtering and reflection from a beryllium surface: Effects of hydrogen isotope mass, impact position and surface binding energy, *Nucl. Fusion* **62**, 066024 (2022).
- [57] J. Steinier, Y. Termonia, and J. Deltour, Smoothing and differentiation of data by simplified least square procedure, *Anal. Chem.* **44**, 1906 (1972).
- [58] O. F. Oxtoby, D. E. Pelinovsky, and I. V. Barashenkov, Travelling kinks in discrete  $\phi^4$  models, *Nonlinearity* **19**, 217 (2006).
- [59] S. V. Dmitriev, A. Khare, P. G. Kevrekidis, A. Saxena, and L. Hadžievski, High-speed kinks in a generalized discrete  $\phi^4$  model, *Phys. Rev. E* **77**, 056603 (2008).
- [60] R. I. Garber and A. I. Fedorenko, Focusing of atomic collisions in crystals, *Sov. Phys. Usp.* **7**, 479 (1965).